Simulation of grout diffusion in fractured rock mass by equivalent seepage lattice elements

Jing Li [a], Xinguang Zhu [b,*], Chun Feng [b], Lixiang Wang [b], Guofeng Han [b], Yiming Zhang [a]

[a] *School of Civil and Transportation Engineering, Hebei University of Technology, Xiping Road 5340, 300401 Tianjin, China*
[b] *Key Laboratory for Mechanics in Fluid Solid Coupling Systems, Institute of Mechanics, Chinese Academy of Sciences, Beijing, China*

ARTICLE INFO

ABSTRACT

There are a large number of discontinuities in underground rock masses with different geometric properties, inducing complex grout diffusion processes. Classical discrete models commonly necessitate fine meshes to explicitly model these discontinuities and result into great computing efforts. In this work, a seepage lattice element model is proposed, which models the fissure seepage by pore seepage in equivalent pipes. We use the new model to study the horizontal grouting cases, considering diffusion as well as solidification processes of Bingham fluid. Some patterns are found: (i) The lattice elements do not need complex discretization which properly capture the grout diffusions processes; (ii) The diffusion of grout will become steady after reaching a specific distance from the injection point where the rock domain full of grout is the diffusion range; (iii) Crack openings, injection pressure and shear strength significantly influence this diffusion range. The proposed method and revealed rules can assist engineers to control the diffusion range and optimize the designs.

1. Introduction

The scale of fractures in underground mining strata varies greatly, which is one of the most important factors affecting the safety and stability of rock mass [1–3]. Horizontal directional grouting [4,5] is widely used to enhance the stability of fractured rock masses. Numerical simulating the grouting processes can help the researchers to optimize the grouting design.

Conventionally, continuum type numerical methods such as finite element method (FEM) [6–9], finite difference method (FDM) [10–13] were used to study the mass transport processes in porous media, which is suitable to capture the pore diffusion but have difficulties to model diffusion in joints and fractures. In recent year, different element/block based models were proposed to capture the diffusions in pores as well as fractures such as continuum equivalent model [14–16], discrete fracture model [17–19] and continuum-discrete hybrid model [20,21]. Most of these models need alignments of discontinuities and element boundaries. When there are many joints and fractures with different scales in the domain, the pre-processing and computing efforts can be great. On the other hand, lattice models were also considered by some researchers [22–25]. For lattice models, the diffusions in pores and fractures are all considered as diffusions in 1D pipes. By equivalently changing the permeability of these pipes, different sizes of pores and fractures are taken into account. Besides, these models can be coupled with spring models to simulate hydro-mechanical processes.

Spring Element Method (SEM) [26–30] is used to construct a physically meaningful spatial mass–spring system in a local coordinate system for representing continuous media systems. It employs a particle–spring system with a specific configuration to describe the constitutive unit system of continuous media. Within the local coordinate system, continuous problems can be effectively addressed. Therefore, porous flow simulations of porous rocks based on a continuous framework are closer to physical and practical mechanical issues.

Compared to Newtonian fluids, some experimental observations have indicated the shear-thinning behavior of Bingham fluids, suggesting their capability to better describe the behavior of mud [31]. The main characteristics of Bingham fluids are their yield stress and plastic viscosity: when subjected to sufficient stress, they exhibit behavior similar to incompressible fluids; when stress is below a threshold, they display solid-like behavior, demonstrating a phenomenon of solidification [32,33]. The flow of Bingham fluids is stabilized by the action of yield stress, and due to this distinctive nature, Bingham fluids find widespread application in the field of drilling mud circulation [34].

Some studies have attempted to simulate karst development by coupling continuum models with pipeline networks, resulting in substantial computational demands [35]. A method is proposed to simulate preferential flow in fracture networks, but due to the relatively simple grid topology, it is challenging to consider local geometric structures [36,

---

* Corresponding author.
E-mail address: zhuxg@imech.ac.cn (X. Zhu).

37]. The existing pipe-network models capture the transmission process through pipes, neglecting mechanical behavior and providing an unclear explanation of the slurry diffusion mechanism [38].

In this study, we fully leverage the advantages of spring elements, introducing time and space-related parameters to comprehensively characterize the entire process of slurry diffusion. Compared to analytical solutions and other theoretical model outcomes, our model demonstrates higher consistency, along with elevated computational efficiency and robustness. In order to study the fluid seepage in underground porous media with complex space, and considering the iterative efficiency and numerical stability in dealing with the seepage problem, an equivalent seepage lattice element model is proposed. The constitutive model of grout is developed to describe the flow and solidification process of Bingham fluid.

- The proposed model establishes an equivalent relationship between the permeability of fractured elements and pore characteristics and after verification, the pore seepage results are found to be consistent with the fracture seepage results, effectively addressing the grouting diffusion problem.
- Using the equivalent seepage lattice element model, the grouting diffusion behavior of the goaf area and surrounding rock mass is analyzed. The grout pressure is found to be directly proportional to crack opening and grouting pressure, while inversely proportional to shear strength.
- The large porosity of the goaf leads to a maximum diffusion velocity of the grout towards the goaf. The pressure at the injection point is the primary factor affecting lateral diffusion, while shear strength is the primary factor affecting vertical diffusion.

The paper is organized as follows: In Section 2, including the seepage spring element algorithm and the fracture-pore equivalent model. In Section 3, the model is verified. In Section 4, the simulation results are presented and discussed, revealing the mechanistic phenomenon of grout diffusion and the main factors affecting the diffusion. Finally, concluding remarks are given in Section 5.

2. Numerical method

2.1. Seepage lattice element

The lattice element method is widely used in the solution of solid mechanics, which can efficiently calculate and flexibly deal with nonlinear and anisotropic large-scale problems [27,29]. We propose to apply the lattice element method to the seepage problem, a linear triangular finite element of any shape as shown in Fig. 1(a), the coordinates of the three nodes are $1(0,0)$, $2(a,0)$ and $3(b,c)$. When calculating the seepage problem, take point 3 as an example, the fluid at point 3 flows to point 1 and point 2, as shown in Fig. 1(b). Set the difference point $4(b,0)$, which point 4 is the interpolation point of 1 and 2, the numbers of the three edges are n_1, n_2 and n_3.

The total pressure corresponding to the three nodes is set in the local coordinate system as p_1, p_2 and p_3 respectively, as shown in Fig. 1(c). Based on Green's formula, the pressure gradient in the x direction of the unit can be expressed as:

$$\frac{\partial p}{\partial x} \approx \frac{1}{S} \iint \frac{\partial p}{\partial x} d_x d_y = \frac{1}{S} \sum_{i=1}^{3} \bar{p}_n \Delta y_n, \tag{1}$$

where, S is the area of the triangle unit, $\bar{p}_n$ is the average pressure on the nth edge, and the calculation formula is:

$$\begin{cases} \bar{p}_1 = (p_1 + p_2)/2, \\ \bar{p}_2 = (p_2 + p_3)/2, \\ \bar{p}_3 = (p_3 + p_1)/2, \end{cases} \tag{2}$$

Δy_n is the difference between the y coordinates of two nodes on the nth edge.

$$\begin{cases} \Delta y_1 = 0, \\ \Delta y_2 = c, \\ \Delta y_3 = -c, \end{cases} \tag{3}$$

Substituting Eqs. (2) to (3) into Eq. (1), we can get:

$$\frac{\partial p}{\partial x} = (p_2 - p_1)/a \tag{4}$$

Similarly, the pressure gradient in the y direction is:

$$\frac{\partial p}{\partial y} = (p_3 - p_4)/c \tag{5}$$

In Eq. (5), $p_4 = \left[\left(1 - \frac{b}{a} \right) p_1 + \frac{b}{a} p_2 \right]$, p_4 is the pressure obtained by interpolation at the foot point.

According to Darcy's law, the flow velocity in two directions of each node of the triangular element is:

$$\begin{cases} v_x = k (p_2 - p_1)/a, \\ v_y = k (p_3 - p_4)/c, \end{cases} \tag{6}$$

where, k is the permeability corresponding to Darcy's law expressed by pressure in pore seepage, which is calculated by dividing the permeability coefficient by the dynamic viscosity. The flow of each node is:

$$\begin{cases} q_1 = ((b-a)v_y - cv_x)/2, \\ q_2 = (cv_x - bv_y)/2, \\ q_3 = (av_y)/2, \end{cases} \tag{7}$$

Fig. 1(c) illustrates the direction of pipeline Q_{12} in the x-axis, which runs from node 1 to node 2. In addition, pipeline Q_{34} flows in the y-axis from node 3 towards the interpolation node 4. The flow rate of the interpolation node 4 is then distributed to node 1 and node 2 in accordance with the proportional coefficient. By substituting Eq. (6) into Eq. (7), it is possible to obtain an expression that is consistent with the solid spring element. This expression provides the relationship between pipe flow and pressure difference.

$$\begin{cases} q_{12} = -ck\Delta p_{12}/2a, \\ q_{34} = -ak\Delta p_{34}/2c, \end{cases} \tag{8}$$

where, q_{12}, q_{34} represent the flow rate of pipeline 1 to 2, 3 to 4, Δp_{12}, Δp_{34} represent the pressure difference of pipeline1 to 2, 3 to 4. In the actual calculation, since point 4 is an interpolation point, q_{34} needs to be assigned to nodes 1 and 2 according to the weight coefficient.

When multiple elements are calculated, it is necessary to superimpose the calculation of the traffic of the common node:

$$Q^E = \sum_{j=1}^{N_e} q_j \tag{9}$$

where, Q^E represents the total flow of pore element nodes, and N_e represents the total number of elements connected to the current node.

2.2. Equivalent fracture-pore model for grout diffusion

Due to the large scale difference of the rock mass in the goaf, the traditional plate flow assumption based on the fracture is not suitable for studying the grout diffusion behavior. Therefore, in order to study the grouting diffusion behavior of the goaf and its surrounding rock mass, it is necessary to develop a numerical calculation method for grouting diffusion based on pore seepage is shown in Fig. 2.

Assuming that the internal pores of the unit are all spherical in shape, the equivalent method diagram of fracture-pore is shown in Fig. 3.
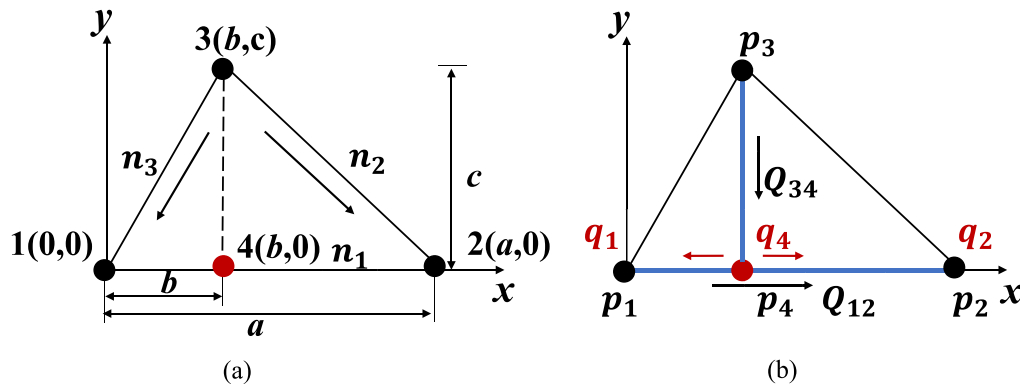
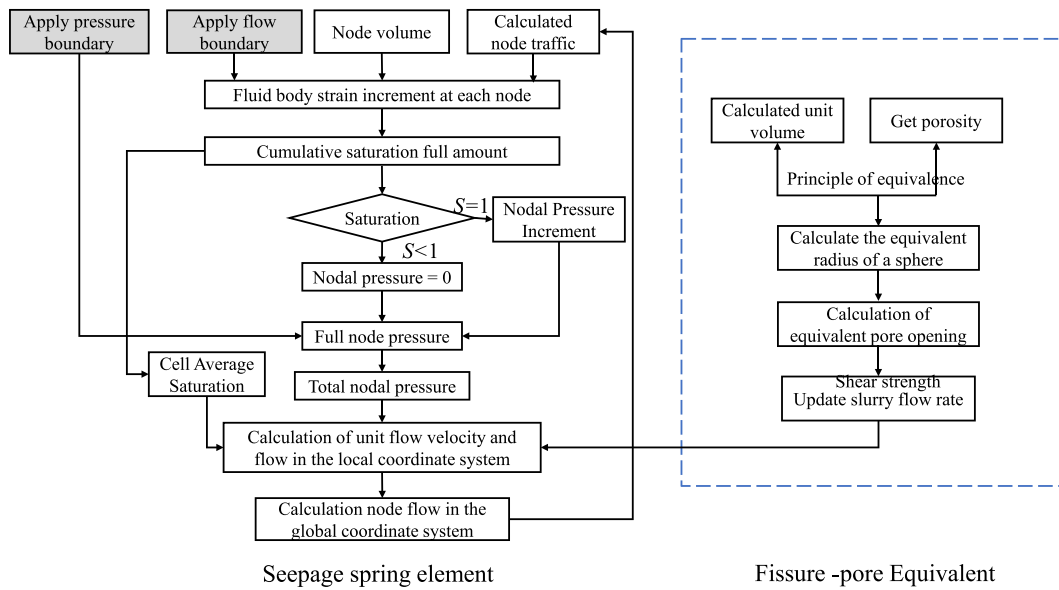**Fig. 1.** Spring element method: (a) Triangle element in local coordinate system, (b) Seepage lattice element pipe.

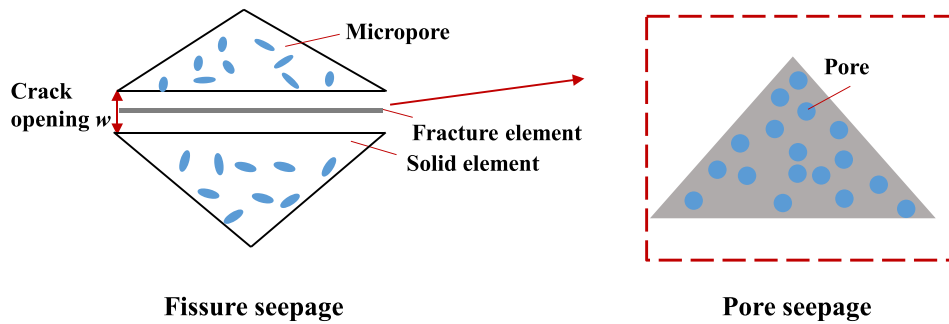**Fig. 2.** Fracture-pore equivalent algorithm flow chart.

Fig. 3. Fracture-pore equivalent diagram.

The pores inside the rock mass are equivalently regarded as uniform spheres with equal radius, and the following formula is obtained from the equal pore volume in the space:

$$\frac{4}{3}\pi r^3 N = nV, \tag{10}$$

where, r is the equivalent radius of the pores, n is the porosity, V is the domain volume, and N is the number of pores. Solve the above formula to get equivalent radius:

$$r = \sqrt[3]{\frac{3nV}{4\pi N}}, \tag{11}$$

Link the crack opening w with the equivalent radius r of the pore, that is:

$$w = 2r = 2\sqrt[3]{\frac{3nV}{4\pi N}}, \tag{12}$$

As a typical Bingham fluid, the grout begins to flow only when it reaches a critical value of the minimum shear stress [39,40]. Below this critical value, the Bingham fluid behaves as an ordinary elastic body. Since the Bingham fluid has higher flow resistance than the Newtonian fluid, the Bingham fluid needs a higher grouting pressure to achieve the same diffusion distance for the two slurries [41].
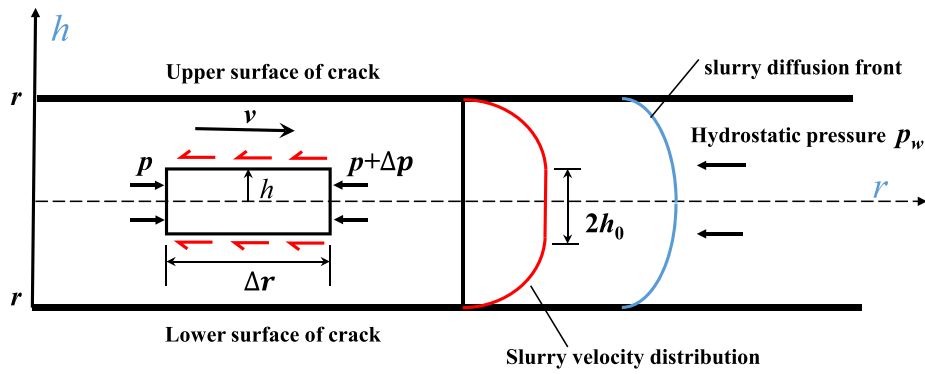
Fig. 4. Bingham fluid model.

As shown in Fig. 4, the Bingham fluid only flows laminarly in parallel fractures along the horizontal direction. At any microelement, the force balance equation of the microelement body can be expressed as:

$$2\tau_s \Delta r + h\Delta p = 0, \tag{13}$$

where, τ_s is the shear strength, between the pipe wall and the grout, it can be expressed as:

$$\tau_s = -\frac{h\Delta p}{2\Delta r}, \tag{14}$$

Based on the equivalent crack opening, the average fluid velocity [31] can be expressed as:

$$\bar{u} = -\frac{\partial p}{\partial x}\frac{w^2}{12\mu}\left[1 - \frac{3Z}{w} + 4\left(\frac{Z}{w}\right)^3\right] \tag{15}$$

where, μ is the dynamic viscosity, w is the crack opening, x is the coordinate component, and the expression of Z is:

$$\bar{u} = -\frac{\partial p}{\partial x}\frac{w^2}{12\mu}\left[1 - \frac{3Z}{w} + 4\left(\frac{Z}{w}\right)^3\right] \tag{16}$$

$$Z = \tau_s\left(\frac{\partial p}{\partial x}\right)^{-1} < \frac{w}{2}, \tag{17}$$

3. Numerical verification

3.1. Verification of fracture-pore equivalent model

Fig. 5(a) and (b) illustrate the results of the verification test where a constant pressure was applied on the left side of the model and the seepage parameters are shown in Table 1. After obtaining the stable calculation, Fig. 5(a) shows the pressure distribution of fracture seepage and pore seepage are same. Further analysis and stabilization resulted in the pressure values of the two methods in different spaces, which were plotted as curves, as shown in Fig. 5(b). The curves show that the pressure of the two calculation methods is zero at $x = 4$ m, and the overall pressure value curves are in good agreement, albeit with slight differences. These differences may be attributed to the random distribution of pores assumed in the pore units in this project, leading to nonlinearity of the pressure gradient caused by the uncertainty of pore positions. Nonetheless, the results indicate that the proposed pore seepage method is reliable and can effectively deal with the grouting diffusion problem in underground porous media with complex space.

3.2. Verifying the grouting models

Validate this model with the proposed Bingham fluid analytical solution by Gustafson [42], and the grout parameters are obtained from the literature, as shown in Table 2. The relationship between penetration diffusion distance and penetration time is as follows:

Table 1
Seepage main parameters.

Material properties	Value
Pressure P (kPa)	500
Crack opening w (m)	1.5×10^{-4}
Permeability k (m^2/(Pa s))	1.67×10^{-7}

Table 2
Parameters for verification simulation.

Parameters	Value
Pressure P (kPa)	30
Crack opening w (m)	5×10^{-3}
Grout density ρ (kg/m^3)	1400
Initial grout viscosity μ (Pa s)	0.04
Yield stress τ_0 (Pa)	1

$$\begin{aligned} I &= I_D \cdot I_{max}, \\ t &= t_D \cdot t_0, \\ I_D &= \sqrt{\theta^2 + 4\theta} - \theta, \\ t_0 &= \frac{6\Delta p \cdot \mu}{\tau_0^2}, \\ I_{max} &= \frac{\Delta pw}{2\tau_0}, \\ \theta &= \frac{t_D}{2\left(0.6 + t_D\right)}, \end{aligned} \tag{18}$$

where t_D and I_D are relative penetration time and relative penetration length, respectively, t_0 is the characteristic grouting time, I_{max} is the maximum grout penetration, and θ is a ratio influenced by t_D.

As shown in Fig. 6, when comparing the simulation results of this model with those of the Unified Pipe-Network Method (UPM) and the analytical solution, it is observed that the diffusion distance along the pore over time is in good agreement. This validates the effectiveness of the injection model proposed in this study.

Zhou et al. [43] established a theoretical model for grouting in saturated homogeneous rock fractures to investigate the variation in the diffusion distance of the grout. In this study, the grout is treated as a Bingham fluid, and the grout parameters are obtained from the literature, as shown in Table 3.

The comparison between numerical results and literature data is shown in Fig. 7. The trend of results from the early to later stages of grouting is quite consistent. It is observed that with a constant grouting pressure, the diffusion distance gradually stabilizes during the later stages of grouting. This indicates that the proposed model can accurately describe the grouting process.
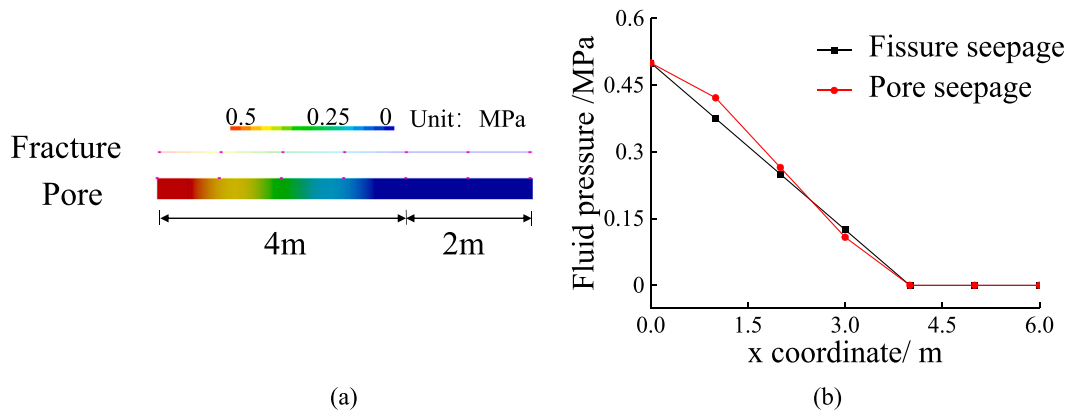
Fig. 5. Verification of fracture-pore equivalent model: (a) The pressure distribution of fracture and pore seepage. (b) Fracture-pore pressure correlation.
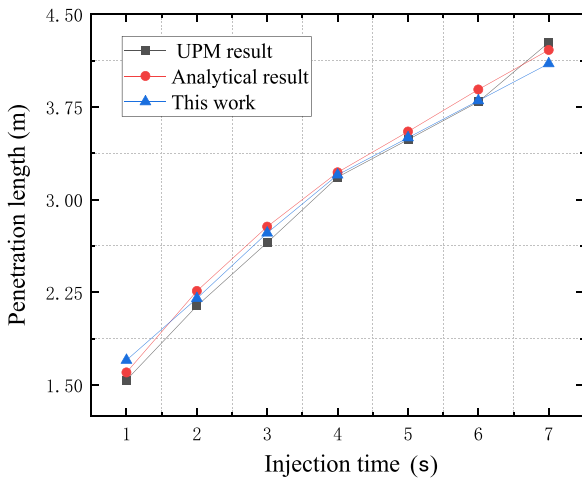

Fig. 6. Comparison of the simulation results of this model with those of the Unified Pipe-Network Method (UPM) and the analytical solution.
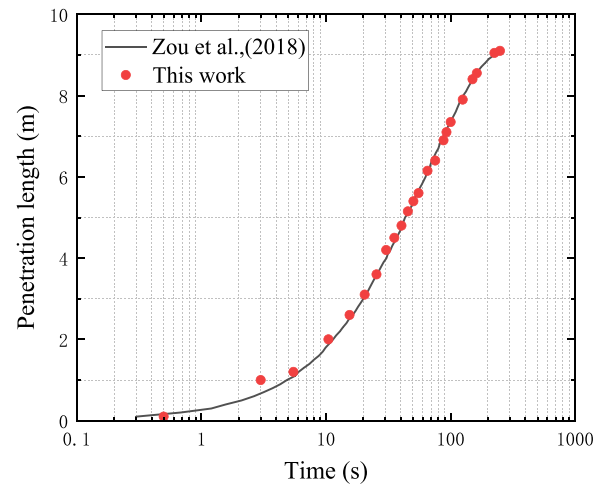

Fig. 7. Comparison of spread distance between theoretical model and numerical results.

Table 3
Parameters for verification simulation.

Parameters	Value
Pressure P (kPa)	100
Crack opening w (m)	1×10^{-3}
Grout density ρ (kg/m³)	1500
Initial grout viscosity μ (Pa s)	0.01
Yield stress τ_0 (Pa)	2

Table 4
Grout parameters.

Fluid density (kg m⁻³)	Bulk modulus (MPa)	Crack opening (mm)	Shear strength (Pa)	Injection pressure (MPa)
		0.15	5	1.25
		0.175	7	1.5
1810	1	0.2	9	2
		0.25	11	2.5

4. Numerical result

Grout pressure, grouting time, shear strength, and crack opening are all crucial factors in guiding grouting design and field engineering practices. They have a significant impact on the diffusion behavior of grout in underground rock formations. By analyzing the grout diffusion behavior using an equivalent fracture-pore seepage model, we can gain valuable insights into how these various parameters influence the process.

4.1. Numerical model of grout diffusion

To investigate the diffusion law of grouting in underground goaf, directional grouting of horizontal holes was used to explore changes within the range of mined-out areas [44], as shown in Fig. 8.he simulation was carried out on an 80 m × 80 m model, divided into four layers of strata: the bottom plate, collapse zone, fissure zone, and curved sinking zone, as shown in Fig. 9(a). To improve accuracy, we employed

a refined mesh in the central region of the model and established the grout parameters listed in Table 4. The injection point was positioned at the center of the model with coordinates (40, 45), while the monitoring point was placed below the injection point at coordinates (40, 60), as shown in Fig. 9(b). In order to accurately simulate the underground grouting environment, we considered porosity as a significant influencing factor, which was set to increase gradually from the goaf, as shown in Fig. 9(c).

4.2. Grout diffusion form

The variation in grout pressure diffusion over time is shown in Fig. 10(a). The grout pressure decreases towards the center. At the initial stage of grouting, the presence of goaf porosity causes the grout velocity to gradually decrease from the injection point downwards, as shown in Fig. 10(b). The upper part of the injection point exhibits a slower average grout velocity compared to the lower part, resulting in a significant increase in downward diffusion of the grout. Over time,
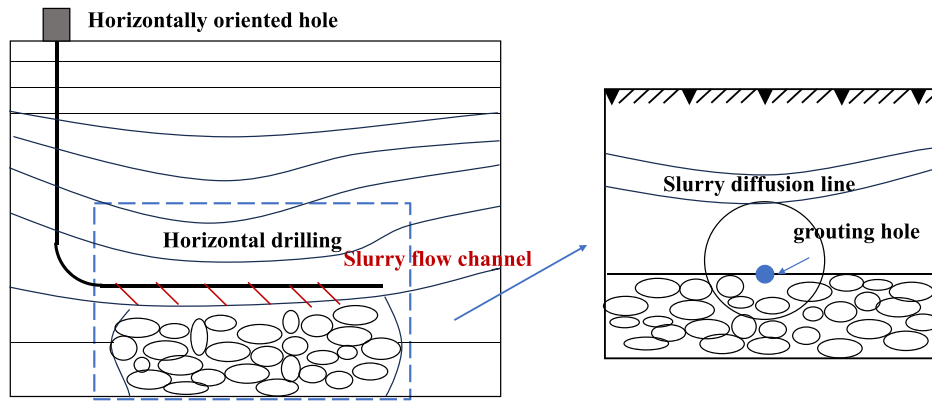
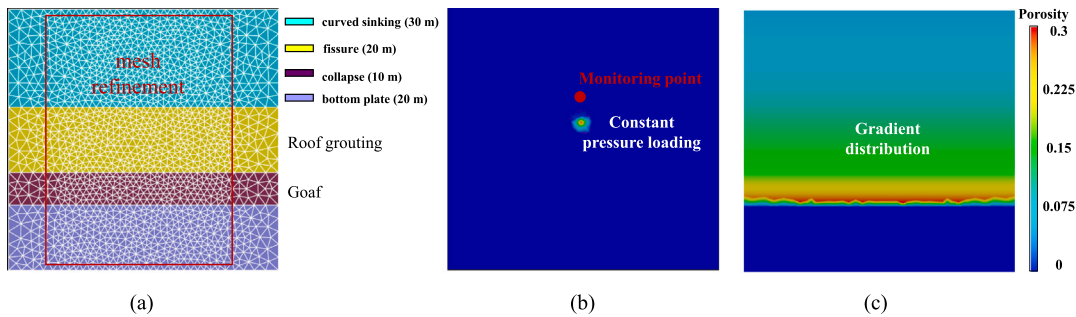**Fig. 8.** Schematic diagram of horizontal drilling grouting.

Fig. 9. Numerical Model of grout Diffusion: (a) Mesh, (b) Boundary Condition Setting, (c) Porosity distribution.
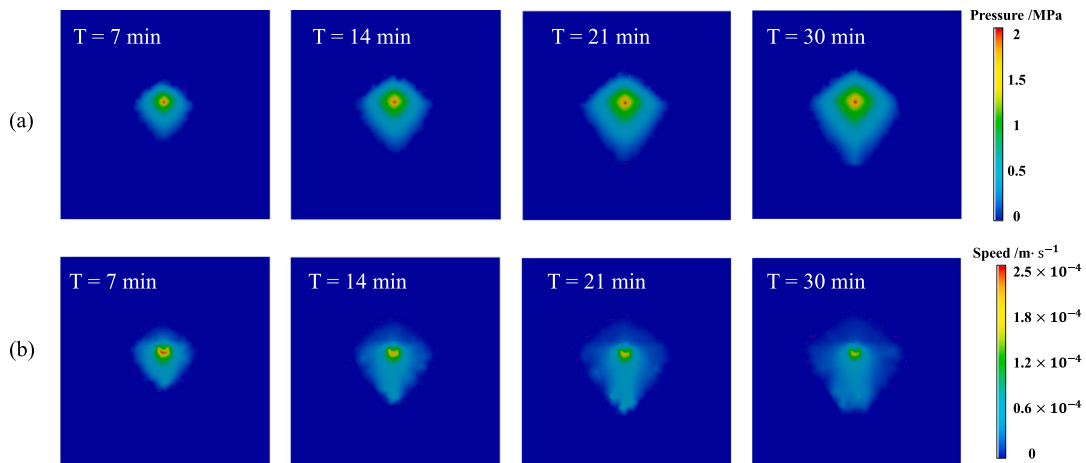

Fig. 10. Grout characteristics at different times: (a) Grout pressure, (b) Maximum speed.

the grout velocity gradually decreases towards the surrounding areas, leading to an expansion of the grout's diffusion range before eventually reaching a stable state.

The static water plane diffusion pattern of the grout in a fixed porosity is shown in Fig. 11. Saturation refers to the volume fraction of grout injected into the pores of the rock mass. To clarify the parameters influenced by slurry diffusion, boundary values are selected for analysis. And as shown in Fig. 11(a), the contour map clearly demonstrates the significant impact of the injection point pressure on the diffusion range of the grout. Specifically, a higher pressure at the injection point results in a greater amount of grout diffusing through the pore channels.

While keeping other parameters constant, we can observe the effect of shear strength, as shown in Fig. 11(b). The diffusion pattern of the grout in the lower part resembles droplets, and an increase in shear

strength leads to higher frictional resistance, consequently reducing both horizontal and vertical diffusion distances.

Likewise, with other parameters maintained at constant levels, we analyzed the grout diffusion cloud map under various crack openings, as shown in Fig. 11(c), found that larger crack openings result in a larger amount of diffusion. The change of grout diffusion shape affected by crack opening is similar to that affected by grouting pressure.

4.3. Pressure distribution law

The pressure applied at the injection point acts as the driving force for grout diffusion in the borehole. By maintaining other parameters at constant values and adjusting the pressure at the injection point, we can observe the corresponding changes, as shown in Fig. 12(a).
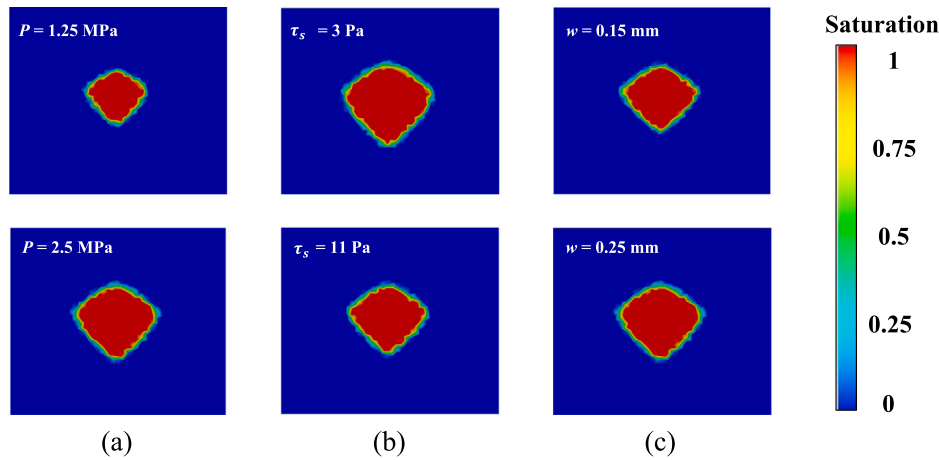
Fig. 11. The morphology of grout diffusion under different parameters: (a) Injection point pressure, (b) Shear strength, (c) Crack opening.
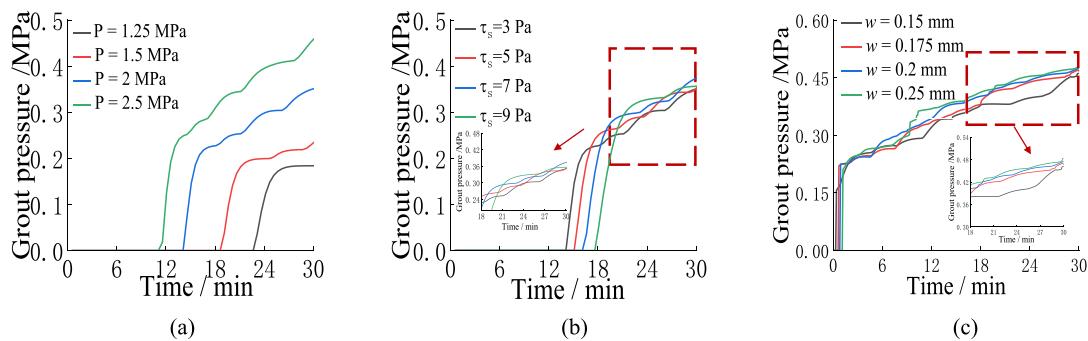

Fig. 12. Grout pressure time-history curves with different parameters: (a) Injection point pressure, (b) Shear strength, (c) Crack opening.

Increasing the pressure at the injection point leads to an elevation in grout pressure at the monitoring point. For example, when the pressure at the injection point is 1.25 MPa, the resulting stable grout diffusion pressure is 0.19 MPa. Similarly, when the injection point pressure is raised to 2.5 MPa, the stable grout diffusion pressure reaches 0.28 MPa. Consequently, under high-pressure conditions, the grout pressure experienced along the pathway is notably higher.

Keeping other parameters constant, we can investigate the influence of shear strength, as shown in Fig. 12(b). The results indicate a positive correlation between pressure loss and slurry shear strength. This implies that higher shear strength leads to lower slurry diffusion pressure. In the initial stages, when the rock mass exhibits relatively high porosity, the slurry has not completely filled the voids. Increasing shear strength delays the onset of slurry pressure generation. As grouting continues, due to the delayed slurry pressure generation caused by higher shear strength, a positive correlation between shear strength and slurry pressure is observed during the pressure attenuation process. During stable grouting, when shear strength surpasses a certain threshold, a negative correlation between shear strength and slurry pressure emerges.

Maintaining other parameters constant, we can investigate the effect of crack aperture on slurry diffusion within the porous medium. The temporal variation of slurry pressure under different crack opening conditions is depicted in Fig. 12(c). In the initial stages of grouting, when the slurry has not fully filled the pores, the differences in slurry pressure among various crack apertures are relatively small. During the pressure attenuation phase, the slurry pressure with a 0.15 mm aperture exhibits more significant deviation, indicating that with smaller apertures, the phenomenon of slurry pressure decay is more pronounced. When grouting stabilizes, the cracks are filled with water, exerting compression on the rock mass. Larger crack apertures accommodate more slurry, resulting in higher slurry pressure.

4.4. Grout diffusion range

Horizontal monitoring points were placed at $y = 35$ m and $y = 60$ m in the x direction. Fig. 13(a)–(c) illustrates the grout pressure distribution under steady-state conditions at various locations. The grout pressure showed a symmetrical distribution with the injection point as the center. Fig. 13(a) displays the changes in grout pressure resulting from modifications in the injection point pressure, while other grout parameters remain constant. Notably, decreasing the injection point pressure leads to a reduction in the transverse diffusion distance of the slurry.

Fig. 13(b) shows the changes in grout pressure when the shear strength is altered while keeping the other parameters constant. Increasing the shear strength leads to a decrease in grout pressure. Moreover, as the vertical coordinate y increases, the grout pressure gradually diminishes until it reaches a stable state.

Fig. 13(c) illustrates the changes in grout pressure when the crack opening is modified, while keeping other parameters constant. It is evident that an increase in crack opening leads to a corresponding increase in grout pressure, accompanied by an expansion of the grout diffusion distance. Notably, the impact of crack opening on the grout diffusion range is more pronounced in the upper part of the injection point. However, at $y = 35$ m, the crack opening has no significant effect on the peak grout pressure. The Fig. 13(a)–(c) show that as the power source of grout diffusion, the grouting pressure is the main factor affecting the lateral diffusion distance.

When comparing the diffusion pressures at $y = 35$ m and $y = 60$ m, it is generally observed that the upper part of the grouting point generally has lower diffusion pressure than the lower part, and the grout diffusion tends to achieve stability more easily. Furthermore, analyzing the vertical diffusion distance of the grout involves examining the grout
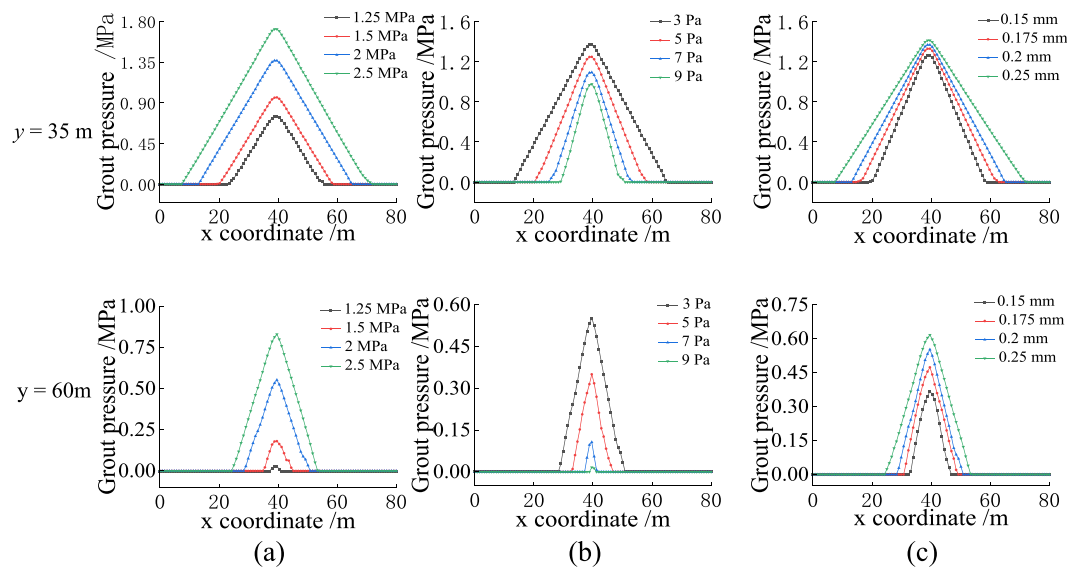
Fig. 13. Mud grout pressure curves with different parameters: (a) Injection point pressure, (b) Shear strength, (c) Crack opening.

pressure at different heights. It can be seen that the attenuation of the vertical grout pressure is most affected by the shear strength. Due to the large porosity of the goaf, the grout gradually flows downward. The distance from the injection point gradually increases during the flow along the path, which is mainly affected by the shear strength along the path.

5. Conclusion

In this paper, an equivalent seepage lattice element model is proposed, and a grout constitutive model to effectively characterize the flow and solidification process of Bingham fluid. The main aim is to address the issue of large-scale variations in underground rock mass engineering. Parametric analysis is conducted on the problem of horizontal hole grouting, allowing for a comprehensive evaluation of grouting diffusion behavior in the goaf and the surrounding rock mass. The findings from our study lead to the following conclusions:

- The equivalent seepage lattice element model establishes an equivalent relationship between fracture unit permeability and pore characteristics. The pore seepage outcomes align well with the fracture seepage pressure diffusion results, effectively dealing with the grouting diffusion problem.
- Due to the high porosity of the goaf, the grout exhibits its maximum diffusion velocity towards the goaf, resulting in a droplet-shaped distribution under the injection point due to the influence of gravity. The grout pressure follows a symmetrical distribution and is directly influenced by the crack opening and grouting pressure, while inversely affected by the shear strength.
- The diffusion pattern of the grout exhibits a symmetrical distribution centered around the grouting point. The transverse diffusion distance is mainly determined by the grouting pressure, and the vertical diffusion distance is mainly affected by the shear strength along the channel.

Declaration of competing interest

The authors declare the following financial interests/personal relationships which may be considered as potential competing interests: Xinguang Zhu reports financial support was provided by Institute of Mechanics Chinese Academy of Sciences. Jing Li reports a relationship with Hebei University of Technology that includes: consulting or advisory. none

Data availability

Data will be made available on request.

References

[1] Liang B, Jiang H, Li J, Gong C. A systematic study of fracture parameters effect on fracture network permeability based on discrete-fracture model employing Finite Element Analyses. J Nat Gas Sci Eng 2016;28:711–22.

[2] Li Y, Chen Y, Jiang Q, Hu R, Zhou C. Performance assessment and optimization of seepage control system: A numerical case study for Kala underground powerhouse. Comput Geotech 2014;55:306–15.

[3] Zheng J, Wang X, Lv Q, Sun H, Guo J. A new determination method for the permeability tensor of fractured rock masses. J Hydrol 2020;585:124811.

[4] Yang Z, Neuweiler I, Méheust Y, Fagerlund F, Niemi A. Fluid trapping during capillary displacement in fractures. Adv Water Resour 2016;95:264–75, Pore scale modeling and experiments.

[5] Hu R, Zhou C, Wu D-S, Yang Z, Chen Y-F. Roughness control on multiphase flow in rock fractures. Geophys Res Lett 2019;46:12002–11.

[6] Schrefler BA, Secchi S, Simoni L. On adaptive refinement techniques in multi-field problems including cohesive fracture. Comput Methods Appl Mech Engrg 2006;195(4):444–61, Adaptive Modeling and Simulation.

[7] Huang M, Jia C-Q. Strength reduction FEM in stability analysis of soil slopes subjected to transient unsaturated seepage. Comput Geotech 2009;36(1):93–101.

[8] xin Jie Y, dong Fu X, Deng G. Treatment of transitional element with the Monte Carlo method for FEM-based seepage analysis. Comput Geotech 2013;52:1–6.

[9] Li X, Li X, Wu Y, Wu L, Yue Z. Selection criteria of mesh size and time step in FEM analysis of highly nonlinear unsaturated seepage process. Comput Geotech 2022;146:104712.

[10] Fukuchi T. Numerical analyses of steady-state seepage problems using the interpolation finite difference method. Soils Found 2016;56(4):608–26.

[11] Yan C, Gao Y, Guo H. A FDEM based 3D discrete mixed seepage model for simulating fluid driven fracturing. Eng Anal Bound Elem 2022;140:447–63.

[12] Tylingo R, Kempa P, Banach-Kopeć A, Mania S. A novel method of creating thermoplastic chitosan blends to produce cell scaffolds by FDM additive manufacturing. Carbohydr Polymers 2022;280:119028.

[13] Li B, Zhang S, Zhang L, Gao Y, Xuan F. Strain sensing behavior of FDM 3D printed carbon black filled TPU with periodic configurations and flexible substrates. J Manuf Process 2022;74:283–95.

[14] Wei W, Jiang Q, Ye Z, Xiong F, Qin H. Equivalent fracture network model for steady seepage problems with free surfaces. J Hydrol 2021;603:127156.

[15] Liu J, Wang J, Gao F, Leung CF, Ma Z. A fully coupled fracture equivalent continuum-dual porosity model for hydro-mechanical process in fractured shale gas reservoirs. Comput Geotech 2019;106:143–60.

[16] kai Chen S, dong He Q, gang Cao J. Seepage simulation of high concrete-faced rockfill dams based on generalized equivalent continuum model. Water Sci Eng 2018;11(3):250–7.

[17] Wang B, Feng Y, Zhou X, Pieraccini S, Scialò S, Fidelibus C. Discontinuous boundary elements for steady-state fluid flow problems in discrete fracture networks. Adv Water Resour 2022;161:104125.

[18] Xue K, Zhang Z, Zhong C, Jiang Y, Geng X. A fast numerical method and optimization of 3D discrete fracture network considering fracture aperture heterogeneity. Adv Water Resour 2022;162:104164.

[19] Yin T, Chen Q. Simulation-based investigation on the accuracy of discrete fracture network (DFN) representation. Comput Geotech 2020;121:103487.

[20] Khoei A, Hosseini N, Mohammadnejad T. Numerical modeling of two-phase fluid flow in deformable fractured porous media using the extended finite element method and an equivalent continuum model. Adv Water Resour 2016;94:510–28.

[21] Xu X, Wu Z, Sun H, Weng L, Chu Z, Liu Q. An extended numerical manifold method for simulation of grouting reinforcement in deep rock tunnels. Tunn Undergr Space Technol 2021;115:104020.

[22] Ma G, Li T, Wang Y, Chen Y. Numerical simulations of nuclide migration in highly fractured rock masses by the unified pipe-network method. Comput Geotech 2019;111:261–76.

[23] Chen Y, Ma G, Li T, Wang Y, Ren F. Simulation of wormhole propagation in fractured carbonate rocks with unified pipe-network method. Comput Geotech 2018;98:58–68.

[24] Ren F, Ma G, Wang Y, Fan L. Pipe network model for unconfined seepage analysis in fractured rock masses. Int J Rock Mech Min Sci 2016;88:183–96.

[25] Ma G, Wang Y, Li T, Chen Y. A mesh mapping method for simulating stress-dependent permeability of three-dimensional discrete fracture networks in rocks. Comput Geotech 2019;108:95–106.

[26] Feng C, Liu X, Lin Q, Li S. A simple particle–spring method for capturing the continuous–discontinuous processes of brittle materials. Eng Anal Bound Elem 2022;139:221–31.

[27] Feng C, Li S, Liu X, Zhang Y. A semi-spring and semi-edge combined contact model in CDEM and its application to analysis of Jiweishan landslide. J Rock Mech Geotech Eng 2014;6(1):26–35.

[28] Zhu X, Feng C, Cheng P, Wang X, Li S. A novel three-dimensional hydraulic fracturing model based on continuum-discontinuum element method. Comput Methods Appl Mech Engrg 2021;383:113887.

[29] Wang X, Feng C, Zhu X, Zhang L, Li S. A half-space based contact detection algorithm for complex blocks. Comput Geotech 2021;135:104168.

[30] Feng C, Li S, Lin Q. A block particle coupled model and its application to landslides. Theor Appl Mech Lett 2020;10(2):79–86.

[31] Chiou J-S, Ng JL. Investigation of Newtonian and non-Newtonian Bingham fluid models for lateral flow simulation of liquefied soil. Ocean Eng 2022;266:112990.

[32] Fusi L, Farina A, Rajagopal KR, Vergori L. Channel flows of shear-thinning fluids that mimic the mechanical response of a Bingham fluid. Int J Non-Linear Mech 2022;138:103847.

[33] De los Reyes JC, González Andrade S. Numerical simulation of two-dimensional Bingham fluid flow by semismooth Newton methods. J Comput Appl Math 2010;235(1):11–32.

[34] Lavrov A. Flow of non-Newtonian fluids in single fractures and fracture networks: Current status, challenges, and knowledge gaps. Eng Geol 2023;321:107166.

[35] Bodin J, Porel G, Delay F, Ubertosi F, Bernard S, de Dreuzy J-R. Simulation and analysis of solute transport in 2D fracture/pipe networks: The SOLFRAC program. J Contam Hydrol 2007;89(1):1–28.

[36] Ubertosi F, Delay F, Bodin J, Porel G. A new method for generating a pipe network to handle channelled flow in fractured rocks. C R Geosci 2007;339(10):682–91.

[37] Ren F, Ma G, Wang Y, Li T, Zhu H. Unified pipe network method for simulation of water flow in fractured porous rock. J Hydrol 2017;547:80–96.

[38] Sun Z, Yan X, Liu R, Xu Z, Li S, Zhang Y. Transient analysis of grout penetration with time-dependent viscosity inside 3D fractured rock mass by unified pipe-network method. Water 2018;10(9).

[39] Zou L, Håkansson U, Cvetkovic V. Analysis of Bingham fluid radial flow in smooth fractures. J Rock Mech Geotech Eng 2020;12(5):1112–8.

[40] Fusi L, Farina A. Peristaltic flow of a Bingham fluid in a channel. Int J Non-Linear Mech 2017;97:78–88.

[41] Basov I, Shelukhin V. Nonhomogeneous incompressible Bingham viscoplastic as a limit of nonlinear fluids. J Non-Newton Fluid Mech 2007;142(1):95–103, Viscoplastic fluids: From theory to application.

[42] Gustafson G, Stille H. Stop criteria for cement grouting. 2005.

[43] Zou L, Håkansson U, Cvetkovic V. Two-phase cement grout propagation in homogeneous water-saturated rock fractures. Int J Rock Mech Min Sci 2018;106:243–9.

[44] Liang J, Du X, Fang H, Du M, Shi M, Gao X, Han Y. Numerical and experimental study of diffusion law of foamed polymer grout in fracture considering viscosity variation of slurry. Tunn Undergr Space Technol 2022;128:104674.